Journal of Genetics and Genomics 46 (2019) 499–503

Contents lists available at ScienceDirect

Journal of Genetics and Genomics

Journal homepage: www.journals.elsevier.com/journal-of-genetics-and-genomics/

Letter to the editor

Evolutionary selection on MDA5 and LGP2 in the chicken preserves antiviral competence in the absence of RIG-I

The pattern recognition receptors (PRRs) act as the first line of defense against pathogens and are common molecular targets in the conflict between viruses and their host (Tan et al., 2018). The RIG-I-like receptors (RLRs), including RIG-I (Yoneyama et al., 2004), MDA5 (Andrejeva et al., 2004), and LGP2 (Saito et al., 2007), are PRRs and reside in the cytoplasm. These proteins recognize the RNA structures of different viral RNA species. All RLRs have an intermediate RNA helicase domain that catalyzes ATP hydrolysis and a C-terminal domain (CTD). RIG-I and MDA5, but not LGP2, contain tandem caspase recruitment domains at their N-termini that can directly interact with the adaptor MAVS (mitochondrial antiviral signaling protein) (Liu and Gao, 2018) to activate downstream signaling. LGP2 cannot activate MAVS by itself, but regulates double-stranded RNA (dsRNA)-stimulated RIG-I and MDA5 signaling (Satoh et al., 2010; Tan et al., 2018). Activation of MAVS results in proinflammatory cytokine and type I interferon (IFN) production through NF-κB and/or IRF3/IRF7 (Ronald and Beutler, 2010; Takeuchi and Akira, 2010).

Despite having shared downstream signaling pathways, RIG-I and MDA5 play non-redundant roles by recognizing largely distinct groups of different viral RNAs. RIG-I is essential for the production of interferons in response to many RNA viruses, including paramyxoviruses (such as Newcastle disease virus [NDV]), influenza virus, and Japanese encephalitis virus, whereas MDA5 recognizes picornavirus (Kato et al., 2006). Although the RLRs are generally well conserved in vertebrates, RIG-I has been lost in the chicken and this genetic alteration has affected the innate immune responses against avian influenza virus (AIV) infection. Inactivation of antiviral genes downstream of RIG-I and attenuation of IFN production conferred susceptibility to AIV (Barber et al., 2010). The chicken MDA5 (chMDA5) was believed to be one of the PRRs responsible for AIV infection and could sense short dsRNA in the absence of RIG-I (Karpala et al., 2011; Hayashi et al., 2014). Consistent with this acquired function of chMDA5, siRNA-mediated knockdown of *chMDA5* decreased *chIFN-β* mRNA level induced by AIV (Karpala et al., 2011; Liniger et al., 2012). chMDA5 had a higher preference for recognizing the short poly(I:C) (0.2–1 kb) than the longer one (1.5–8 kb) (Hayashi et al., 2014). The chicken LGP2 (chLGP2) could positively regulate chMDA5-dependent IFN production (Liniger et al., 2012). These observations have indicated that chMDA5 and chLGP2 might compensate for the loss of function of RIG-I in the AIV-induced antiviral signaling pathway (Karpala et al., 2011; Liniger et al., 2012; Hayashi et al., 2014). In addition, chMDA5 played an antiviral role in NDV (Li et al., 2016) and a truncated chMDA5 (1–483 aa) could enhance the immune efficacy of inactivated NDV vaccine (Han et al., 2019). Subsequent study identified that the viral V protein from NDV inhibited IFN expression through interaction with MDA5 (Childs et al., 2007). Recent structural analyses have shown that chMDA5-dsRNA complex structures have a head-to-head packing on short dsRNAs, and chLGP2-dsRNA structures exhibit a RIG-I-like end binding through its CTD and helicase domain, providing further mechanistic insights into the recognition of virus RNAs by chMDA5 and chLGP2 (Uchikawa et al., 2016).

To address whether pathogen-mediated evolution could drive the functional diversity of the RLR genes in the chicken lineage due to the loss of *RIG-I* (Barber et al., 2010), we compared the chicken, mallard, zebrafish, dog, and cow gene sequences (Table S1) and used the branch model tests implemented by the phylogenetic analysis by maximum likelihood (PAML) (Yang, 2007) (Table S2) to calculate the average nonsynonymous substitution/synonymous substitution rate ($d\ N/d\ S$, also known as ω) for *MDA5* and *LGP2*. *chMDA5* was found to have undergone positive selection in the chicken ($P = 0.014$; Table S2). We also evaluated the positive selection signals by using the branch-site models implemented in the PAML (Yang, 2007). We found that *chLGP2* experienced a positive selection (*chLGP2*, $P = 0.017$; Table S3). We further identified one potentially positively selected site (PSS) in chMDA5 and three PSSs in chLGP2 (Table S3) based on the Bayes Empirical Bayes analysis (Yang et al., 2005).

We tested whether chMDA5 or chLGP2 can sense NDV in chicken DF-1 cells and compensate for the loss of RIG-I, which specifically recognizes NDV (Kato et al., 2006). We used the previously reported method (Xu et al., 2016) to isolate MDA5-associated RNA from the NDV-infected cells. We immunoprecipitated (IP) chMDA5 from the NDV-infected DF-1 cells transiently overexpressing chMDA5 protein (Fig. 1A), extracted RNA from the precipitates, and analyzed its stimulatory activity on *chIFN-β* induction (Fig. 1B). Importantly, we found RNA associated with the chMDA5 precipitates, but not with IgG control precipitates, significantly stimulated the chIFN-β luciferase (chIFN-β-Luc) reporter activity (Fig. 1B *upper*) and the *chIFNB1* mRNA expression in the DF-1 cells (Fig. 1B *below*). We performed a similar RNA-IP assay for chLGP2 (Fig. 1C) and extracted RNA from the precipitates. Consistently with the result for chMDA5 overexpression, the chLGP2-associated RNA could activate the chIFN-β-Luc reporter activity (Fig. 1D *upper*) and induced *chIFNB1* mRNA expression in the DF-1 cells (Fig. 1D *below*). The chMDA5-chLGP2-associated RNAs from the DF-1 cells with overexpression of chLGP2 and chMDA5 in the presence of NDV infection could also activate the chIFN-β-Luc reporter and the *chIFNB1* mRNA expression (Fig. 1E and F). All these results suggested that chMDA5 and chLGP2 can work

https://doi.org/10.1016/j.jgg.2019.10.001

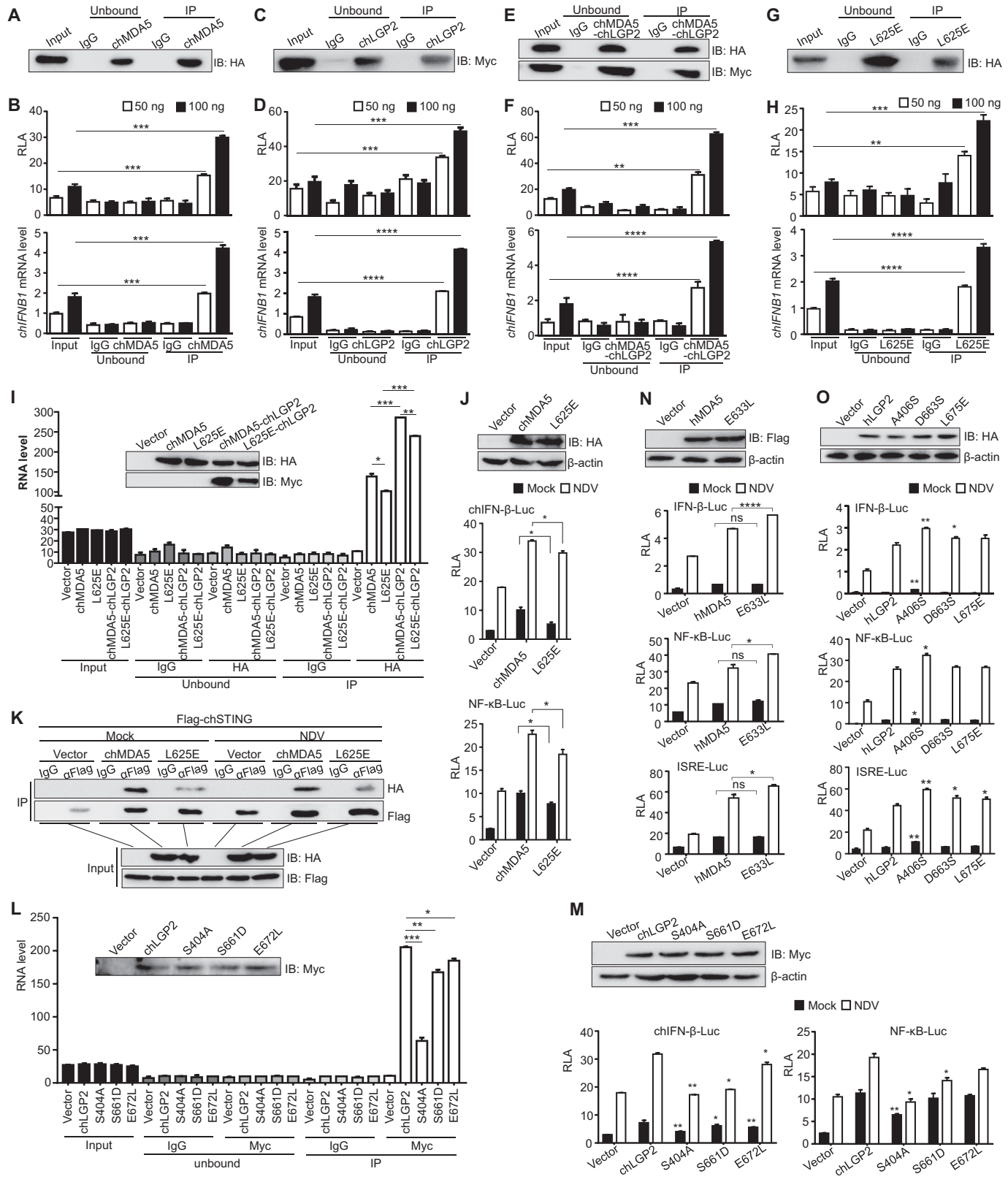

Fig. 1. Functional characterization of the positively selected sites in chMDA5 and chLGP2. **A** and **B**: chMDA5 pull-down captures agonistic RNAs from NDV-infected cells. DF-1 cells (1×10^8) were transfected with 30 μg of HA-tagged chMDA5 expression vector and were cultured for 24 h, then infected by NDV (MOI = 1) for 16 h before harvesting for RNA-IP assays. **A**: Precipitation efficiency was verified by immunoblotting with the anti-HA antibody. **B**: The RNAs from NDV-infected DF-1 cells overexpressing HA-tagged chMDA5 (input), RNAs associated with chMDA5 or IgG immunoprecipitate (IP), or RNAs remaining after chMDA5 or Ig G precipitations (unbound) were used to stimulate the chIFN-β-Luc reporter activity (*upper*) and to induce the *chIFNB1* mRNA expression (*below*). **C** and **D**: chLGP2 pull-down captures agonistic RNAs from NDV-infected cells. **E** and **F**: chMDA5-chLGP2 pull-down captures agonistic RNAs from NDV-infected cells. For the transfection, HA-tagged chMDA5 (29 μg) and Myc-tagged chLGP2 (1 μg) were used. **G** and **H**: chMDA5 mutant L625E pull-down captures agonistic RNA from NDV-infected cells. The procedure in **C**–**H** was similar to that in **A** and **B**. **I**: Quantification of viral RNA bound by the HA-tagged proteins

independently, or together, to bind NDV RNA.

So as to determine whether the PSS in chMDA5 has an acquired function to sense NDV, we swapped the leucine (Leu) at the 625th position back to the evolutionarily conserved glutamate (Glu) (mutant L625E) (Fig. S1), in the DECH helicase domain of MDA5 (Fig. S2A and B). The chMDA5 mutant L625E could sense NDV in our assay (Fig. 1G and H). We measured the level of NDV viral RNA by using quantitative real-time PCR (qRT-PCR) and confirmed the chMDA5 mutant L625E had a slightly weaker binding affinity to viral RNA as compared with the wild type (Fig. 1I). When chLGP2 was co-overexpressed with chMDA5, the chMDA5-chLGP2 combination had the highest ability to bind NDV RNA. The chMDA5 mutant L625E-chLGP2 combination had a weaker binding affinity to NDV RNA than that of chMDA5-chLGP2, but still higher than that of chMDA5 or chMDA5 mutant L625E alone (Fig. 1I). This result suggested that chLGP2 has a positive enhancing effect on the chMDA5-mediated signaling pathway. The roles of chMDA5 mutant L625E and chLGP2 were further confirmed by using a luciferase reporter assay. When we transfected expression vector for chMDA5 or its mutant L625E into DF-1 cells, the chMDA5 significantly induced the chIFN-β and NF-κB-dependent luciferase activities in DF-1 cells with or without NDV infection (Fig. 1J), whereas chMDA5 mutant L625E had an inferior induction effect on the chIFN-β-Luc and NF-κB-Luc activities (Fig. 1J). We obtained a similar result for a relatively higher stimulation effect of chMDA5 than chMDA5 mutant L625E in response to AIV infection (Fig. S2C).

As the chMDA5 could interact with chicken STING (chSTING/MITA/TMEM173/MYPS/ERIS (Motwani et al., 2019)) to enhance antiviral activity (Cheng et al., 2015), we examined whether chMDA5 and its mutant differentially controlled the chSTING-mediated signaling in the DF-1 cells on NDV infection. Consistent with previous observation (Cheng et al., 2015), our IP assay showed that chMDA5 could interact with chSTING (Fig. 1K). The chMDA5 mutant L625E had a weaker interaction with chSTING than that of chMDA5 and chSTING, regardless of NDV infection (Fig. 1K). These results showed that a single positively selected residue change in the chMDA5 has the capacity to modulate the NDV-triggered innate immune signaling.

We swapped the three PSSs (serine at the 404th position in the DECH helicase domain, serine at the 661th and glutamic acid at the 672nd in the RD domain of chLGP2; Figs. S3, S4A and S4B) in the chLGP2 back to the evolutionarily conserved alanine (mutant S404A), aspartic acid (mutant S661D), and leucine (mutant E672L), respectively (Fig. S3). Mutations at the three PSSs in chLGP2 affected their binding capability with NDV RNA (Fig. 1L): mutant S404A had the most striking effect to abolish this capability, whereas mutants S661D and E672L had a weaker binding capability to NDV RNA than shown by the wild type (Fig. 1L). This result was validated by the luciferase assays, in which chLGP2 mutants had a lower ability to induce the chIFN-β- and NF-κB-dependent luciferase activities as compared with the chLGP2 wild type in DF-1 cells, with or without NDV infection (Fig. 1M). We obtained similar results with these mutants in response to AIV infection (Fig. S4C). Taken together, these results suggested that the PSSs in chLGP2 are critical in sensing NDV.

The PSSs in chMDA5 and chLGP2 are all located in critical domains: Leu625 in chMDA5 is located in a β-helix external to the cavity that binds RNA in the DECH box helicase domain (Hel2i), which pivots around its contact with the CTD (Uchikawa et al., 2016); Ser404 in chLGP2 is located in the DECH box helicase domain (Hel 2) and is important for the structure conformation change between the closed state (without dsRNA) and the semiclosed state (with dsRNA), as well as for ATP binding and hydrolysis activity (Uchikawa et al., 2016). The Ser661 and Glu672 in chLGP2 are located in the RD domain, which is structurally similar to that of RIG-I, favors dsRNA binding (Pippig et al., 2009), and provides a less hydrophobic α-helix side chain to form a stable electrostatic interaction with dsRNA. Based on these structural insights, we expected the introduction of these PSSs in chMDA5 and chLGP2 into human homologues would have a similar enhanced antiviral effect as observed in the chicken. We found that hMDA5 E633L (corresponding to chMDA5 Leu625) significantly potentiated the IFN-β-Luc, NF-κB-Luc, and ISRE-Luc activity against NDV as compared with wild-type hMDA5 in HEK293 cells (Fig. 1N). However, we found no difference of the reporter luciferase activities between wild-type hMDA5 and mutant hMDA5 E633L in the mock group (Fig. 1N). This pattern was different from that of wild-type chMDA5 and its mutant L625E, in that mutant L625E had an inferior induction effect than chMDA5 on the chIFN-β-Luc and NF-κB-Luc activities with or without NDV infection (Fig. 1J). We speculated that different patterns for chicken and human MDA5 and their mutants might be caused by species and structure differences, as chMDA5 was shorter than the hMDA5 (Wu et al., 2013) due to a deletion of 17 residues between helixes α12 and α13 of Hel2i (Uchikawa et al., 2016). We performed a gain-of-function analysis by introducing a mutation at the equivalent positions in hLGP2. The hLGP2 mutant A406S significantly induced the IFN-β-Luc, NF-κB-Luc and ISRE-Luc activity as compared with wild-type hLGP2 in HEK293 cells, with or without NDV infection (Fig. 1O). The other two hLGP2 mutants, D663S and L675E, had a similar up-regulating effect, although it was not as striking as that of mutant A406S. These results suggested that the enhanced antiviral effect endowed by the PSSs is conserved in different species because of their critical structural resemblances.

Previous studies on the evolutionary process and imprint of RLRs showed that the RLRs might have originated before the emergence of vertebrates and were rapidly diversified (Mukherjee et al., 2014). However, there were several lineage-specific losses of the *RIG-I* gene in some species, such as some fish species (Biacchesi et al., 2009), the chicken (Barber et al., 2010), and the Chinese tree shrew (Fan et al., 2013, Fan et al., 2019). The recurrent loss of RIG-I in different species implied that RIG-I might have undergone dramatic gene turnover (gain and loss) during vertebrate evolution, which was commonly found for immune genes (Daugherty and

from the NDV-infected DF-1 cells. *Top inserted section*: immunoblots showing HA-tagged chMDA5, L625E, chMDA5-chLGP2, and L625E-chLGP2 in RNA-IP. *Bottom*: measurement of the NDV RNA level by using the quantitative real-time PCR in empty vector, chMDA5, chMDA5 L625E, chMDA5-chLGP2 and chMDA5 L625E-chLGP2, and IgG immunoprecipitates. **J**: Different activation effects of chMDA5 and mutant L625E on the chIFN-β-Luc and NF-κB-Luc reporters. *Top*: Immunoblots showing successful overexpression of HA-tagged chMDA5 and L625E in DF-1 cells (1×10^4), which were transfected with the respective reporter vector (100 ng), TK (10 ng, as an inner control) and indicated expression vector (400 ng) for 36 h. Cells were left uninfected (mock) or infected with NDV (MOI = 1) for 12 h before harvesting for luciferase analysis (*bottom*). **K**: The interaction between chMDA5 L625E and chSTING was weaker than that of chMDA5 and chSTING. The DF-1 cells (1×10^7) were transfected with Flag-chSTING expression vector (5 μg) and expression vector for HA-chMDA5 or L625E mutant (each 5 μg) or empty vector for 24 h, then were infected without (mock) or with NDV (MOI = 1) for 16 h before harvested for immunoprecipitation assays. **L**: Quantification of viral RNA bound by the Myc-tagged chLGP2 and its mutants (S404A, S661D and E672L) from the NDV-infected DF-1 cells. The procedure was similar to that **I**. **M**: Different activation effects of chLGP2 and its mutants on the chIFN-β-Luc and NF-κB-Luc reporters in DF-1 cells. **N** and **O**: Different activation effects of hMDA5, hLGP2 and related mutants on the IFN-β-Luc, NF-κB-Luc and ISRE-Luc reporters in HEK293 cells. The procedure in **M**–**O** was similar to that in **J**. The relative *chIFNB1* mRNA level was normalized by *chGAPDH*. Data are representative of three independent experiments. ns, not significant, $^{*}P < 0.05$, $^{**}P < 0.01$, $^{***}P < 0.0001$, $^{****}P < 0.00001$, Student's *t*-test. For each comparison between hLGP2 and its mutant under the mock or NDV infection condition in **O**, the significance was labeled on the top of the bar. Bars represent mean ± SEM. RLA, relative luciferase activity; NDV, Newcastle disease virus.

Malik, 2012), such as *APOBEC3* (Munk et al., 2012), *PARP14* and *PARP15* (Daugherty et al., 2014). Nonetheless, the evolutionary catastrophe of the RIG-I deficiency would have an effect on the other RLRs, so as to acquire new function to compensate the disadvantage of RIG-I deficiency. As shown in this study, chMDA5 and chLGP2 could sense NDV (Fig. 1A–F), which was presumably done by RIG-I (Kato et al., 2006). This result was in general agreement with the trade-off effect on immune genes due to the long-term arms race between host and viruses (Daugherty and Malik, 2012).

The protein residues evolved under the positive selection were expected to be directly engaged in a constant arms race with pathogens (Daugherty and Malik, 2012). We provided the first-hand data to show that the PSSs in chMDA5 and chLGP2 endowed a higher antiviral effect, which might help to compensate for the role lost through the absence of RIG-I. This result was further confirmed by the higher antiviral effect of the artificial mutants of human MDA5 and LGP2 bearing the chicken PSSs (Fig. 1N–O). A balanced immune activity is needed for the maintenance of homeostasis in the human body. In the presence of RIG-I, the mutations in MDA5 and LGP2, as seen in the chicken, would increase immunity activity, and might cause immune dysfunction and affect the susceptibility to infectious diseases. Indeed, we found no mutations at the PSSs in LGP2 in the available human data sets (Table S4). This result was in agreement with a notion that genes that abnormally enhance immune activity would lead to human diseases and be lost from the population by selection (Brodin and Davis, 2017). Interestingly, we found that the equivalent PSS residue in hMDA5, p.Glu633Asp, was specifically present in East Asians with a minor allele frequency ranging from 0.001 to 0.006 (Table S4). We speculate that these subjects would be more susceptible to autoimmune diseases but may have a higher resistance to infectious diseases because this mutant has a higher antiviral activity. Future study will be needed to confirm this speculation.

The chicken (Galliformes) probably diverged from the Primates about 112 million years ago (Kumar and Hedges, 1998), whereas the tree shrew (Scandentia) diverged from the Primates around 90 million years ago (Fan et al., 2013). It is intriguing that both species had followed the same evolutionary pattern to compensate for the lost RIG-I by endowing additional function for MDA5 and LGP2 (Xu et al. (2016) and this study). There are several key questions stemmed from this study: How did evolution shape this pattern? Did the PSSs occur before or after the loss of RIG-I? Given the importance of RIG-I, we would expect that it cannot be lost unless the function had already become redundant. On this point, we would expect that the PSSs occurred before the loss of RIG-I. Further focused study will be needed to clarify this issue.

In short, we provided an evolutionary analysis and functional evidence to confirm that chMDA5 and chLGP2 have undergone positive selection to acquire additional function to sense NDV and to enhance the NDV-induced antiviral signaling pathway, which provided a functional replacement for the lost RIG-I. The positive selection targeted sites were located at the RNA-binding interface in both chMDA5 and chLGP2, which are critical for sensing NDV infection. Our results uncovered a previously unknown evolutionary signal in response to the loss of RIG-I in the chicken, and provided a rare example for understanding the functional evolutionary path of gene loss and the compensatory mechanism in the innate immune system.

Acknowledgments

We thank Ian Logan for critical comments and language editing for this manuscript. We are grateful to Dr. Hui Yang for helpfully discussion. This work was supported by the National Natural Science Foundation of China (U1402224 and 31700155), Yunnan Province (2016FB018), Sichuan Province (2017JZ0033) and “the Dawn of West China Talent Training Program of Chinese Academy of Sciences”.

Supplementary data

Supplementary data to this article can be found online at https://doi.org/10.1016/j.jgg.2019.10.001.

References

Andrejeva, J., Childs, K.S., Young, D.F., Carlos, T.S., Stock, N., Goodbourn, S., Randall, R.E., 2004. The V proteins of paramyxoviruses bind the IFN-inducible RNA helicase, mda-5, and inhibit its activation of the *IFN-beta* promoter. Proc. Natl. Acad. Sci. U. S. A. 101, 17264–17269.

Barber, M.R., Aldridge Jr., J.R., Webster, R.G., Magor, K.E., 2010. Association of RIG-I with innate immunity of ducks to influenza. Proc. Natl. Acad. Sci. U. S. A. 107, 5913–5918.

Biacchesi, S., LeBerre, M., Lamoureux, A., Louise, Y., Lauret, E., Boudinot, P., Bremont, M., 2009. Mitochondrial antiviral signaling protein plays a major role in induction of the fish innate immune response against RNA and DNA viruses. J. Virol. 83, 7815–7827.

Brodin, P., Davis, M.M., 2017. Human immune system variation. Nat. Rev. Immunol. 17, 21–29.

Cheng, Y., Sun, Y., Wang, H., Yan, Y., Ding, C., Sun, J., 2015. Chicken STING mediates activation of the *IFN* gene independently of the *RIG-I* gene. J. Immunol. 195, 3922–3936.

Childs, K., Stock, N., Ross, C., Andrejeva, J., Hilton, L., Skinner, M., Randall, R., Goodbourn, S., 2007. mda-5, but not RIG-I, is a common target for paramyxovirus V proteins. Virology 359, 190–200.

Daugherty, M.D., Malik, H.S., 2012. Rules of engagement: molecular insights from host-virus arms races. Annu. Rev. Genet. 46, 677–700.

Daugherty, M.D., Young, J.M., Kerns, J.A., Malik, H.S., 2014. Rapid evolution of PARP genes suggests a broad role for ADP-ribosylation in host-virus conflicts. PLoS Genet. 10, e1004403.

Fan, Y., Huang, Z.Y., Cao, C.C., Chen, C.S., Chen, Y.X., Fan, D.D., He, J., Hou, H.L., Hu, L., Hu, X.T., Jiang, X.T., Lai, R., Lang, Y.S., Liang, B., Liao, S.G., Mu, D., Ma, Y.Y., Niu, Y.Y., Sun, X.Q., Xia, J.Q., Xiao, J., Xiong, Z.Q., Xu, L., Yang, L., Zhang, Y., Zhao, W., Zhao, X.D., Zheng, Y.T., Zhou, J.M., Zhu, Y.B., Zhang, G.J., Wang, J., Yao, Y.G., 2013. Genome of the Chinese tree shrew. Nat. Commun. 4, 1426.

Fan, Y., Ye, M.S., Zhang, J.Y., Xu, L., Yu, D.D., Gu, T.L., Yao, Y.L., Chen, J.Q., Lv, L.B., Zheng, P., Wu, D.D., Zhang, G.J., Yao, Y.G., 2019. Chromosomal level assembly and population sequencing of the Chinese tree shrew genome. Zool. Res. 40, 506–521.

Han, Q., Gao, X., Chu, Z., Wang, X., Eisa Addoma Adam, F., Zhang, S., Jia, Y., Qiu, X., Wang, X., Yang, Z., 2019. Truncated chicken MDA5 enhances the immune response to inactivated NDV vaccine. Vet. Immunol. Immunopathol. 208, 44–52.

Hayashi, T., Watanabe, C., Suzuki, Y., Tanikawa, T., Uchida, Y., Saito, T., 2014. Chicken MDA5 senses short double-stranded RNA with implications for antiviral response against avian influenza viruses in chicken. J. Innate Immun. 6, 58–71.

Karpala, A.J., Stewart, C., McKay, J., Lowenthal, J.W., Bean, A.G., 2011. Characterization of chicken Mda5 activity: regulation of IFN-beta in the absence of RIG-I functionality. J. Immunol. 186, 5397–5405.

Kato, H., Takeuchi, O., Sato, S., Yoneyama, M., Yamamoto, M., Matsui, K., Uematsu, S., Jung, A., Kawai, T., Ishii, K.J., Yamaguchi, O., Otsu, K., Tsujimura, T., Koh, C.S., Reis e Sousa, C., Matsuura, Y., Fujita, T., Akira, S., 2006. Differential roles of MDA5 and RIG-I helicases in the recognition of RNA viruses. Nature 441, 101–105.

Kumar, S., Hedges, S.B., 1998. A molecular timescale for vertebrate evolution. Nature 392, 917–920.

Li, R., Guo, K., Liu, C., Wang, J., Tan, D., Han, X., Tang, C., Zhang, Y., Wang, J., 2016. Strong inflammatory responses and apoptosis in the oviducts of egg-laying hens caused by genotype VIId Newcastle disease virus. BMC Vet. Res. 12, 255.

Liniger, M., Summerfield, A., Zimmer, G., McCullough, K.C., Ruggli, N., 2012. Chicken cells sense influenza A virus infection through MDA5 and CARDIF signaling involving LGP2. J. Virol. 86, 705–717.

Liu, B., Gao, C., 2018. Regulation of MAVS activation through post-translational modifications. Curr. Opin. Immunol. 50, 75–81.

Motwani, M., Pesiridis, S., Fitzgerald, K.A., 2019. DNA sensing by the cGAS-STING pathway in health and disease. Nat. Rev. Genet. 20, 657–674.

Mukherjee, K., Korithoski, B., Kolaczkowski, B., 2014. Ancient origins of vertebrate-specific innate antiviral immunity. Mol. Biol. Evol. 31, 140–153.

Munk, C., Willemsen, A., Bravo, I.G., 2012. An ancient history of gene duplications, fusions and losses in the evolution of APOBEC3 mutators in mammals. BMC Evol. Biol. 12, 71.

Pippig, D.A., Hellmuth, J.C., Cui, S., Kirchhofer, A., Lammens, K., Lammens, A., Schmidt, A., Rothenfusser, S., Hopfner, K.-P., 2009. The regulatory domain of the RIG-I family ATPase LGP2 senses double-stranded RNA. Nucleic Acids Res. 37, 2014–2025.

Ronald, P.C., Beutler, B., 2010. Plant and animal sensors of conserved microbial signatures. Science 330, 1061–1064.

Saito, T., Hirai, R., Loo, Y.M., Owen, D., Johnson, C.L., Sinha, S.C., Akira, S., Fujita, T., Gale Jr., M., 2007. Regulation of innate antiviral defenses through a shared repressor domain in RIG-I and LGP2. Proc. Natl. Acad. Sci. U. S. A. 104, 582–587.
Satoh, T., Kato, H., Kumagai, Y., Yoneyama, M., Sato, S., Matsushita, K., Tsujimura, T., Fujita, T., Akira, S., Takeuchi, O., 2010. LGP2 is a positive regulator of RIG-I- and MDA5-mediated antiviral responses. Proc. Natl. Acad. Sci. U. S. A. 107, 1512–1517.
Takeuchi, O., Akira, S., 2010. Pattern recognition receptors and inflammation. Cell 140, 805–820.
Tan, X., Sun, L., Chen, J., Chen, Z.J., 2018. Detection of microbial infections through innate immune sensing of nucleic acids. Annu. Rev. Microbiol. 72, 447–478.
Uchikawa, E., Lethier, M., Malet, H., Brunel, J., Gerlier, D., Cusack, S., 2016. Structural analysis of dsRNA binding to anti-viral pattern recognition receptors LGP2 and MDA5. Mol. Cell 62, 586–602.
Wu, B., Peisley, A., Richards, C., Yao, H., Zeng, X., Lin, C., Chu, F., Walz, T., Hur, S., 2013. Structural basis for dsRNA recognition, filament formation, and antiviral signal activation by MDA5. Cell 152, 276–289.
Xu, L., Yu, D., Fan, Y., Peng, L., Wu, Y., Yao, Y.G., 2016. Loss of RIG-I leads to a functional replacement with MDA5 in the Chinese tree shrew. Proc. Natl. Acad. Sci. U. S. A. 113, 10950–10955.
Yang, Z., 2007. PAML 4: phylogenetic analysis by maximum likelihood. Mol. Biol. Evol. 24, 1586–1591.
Yang, Z., Wong, W.S., Nielsen, R., 2005. Bayes empirical bayes inference of amino acid sites under positive selection. Mol. Biol. Evol. 22, 1107–1118.
Yoneyama, M., Kikuchi, M., Natsukawa, T., Shinobu, N., Imaizumi, T., Miyagishi, M., Taira, K., Akira, S., Fujita, T., 2004. The RNA helicase RIG-I has an essential function in double-stranded RNA-induced innate antiviral responses. Nat. Immunol. 5, 730–737.

Ling Xu
Key Laboratory of Animal Models and Human Disease Mechanisms of the Chinese Academy of Sciences & Yunnan Province, Kunming Institute of Zoology, Kunming, Yunnan, 650223, China

Center for Excellence in Animal Evolution and Genetics, Chinese Academy of Sciences, Kunming, Yunnan, 650223, China

Dandan Yu
Key Laboratory of Animal Models and Human Disease Mechanisms of the Chinese Academy of Sciences & Yunnan Province, Kunming Institute of Zoology, Kunming, Yunnan, 650223, China

Center for Excellence in Animal Evolution and Genetics, Chinese Academy of Sciences, Kunming, Yunnan, 650223, China

Yu Fan
Key Laboratory of Animal Models and Human Disease Mechanisms of the Chinese Academy of Sciences & Yunnan Province, Kunming Institute of Zoology, Kunming, Yunnan, 650223, China

Center for Excellence in Animal Evolution and Genetics, Chinese Academy of Sciences, Kunming, Yunnan, 650223, China

Yi-Ping Liu
Farm Animal Genetic Resources Exploration and Innovation Key Laboratory of Sichuan Province, Sichuan Agricultural University, Chengdu, Sichuan, 611130, China

Yong-Gang Yao*
Key Laboratory of Animal Models and Human Disease Mechanisms of the Chinese Academy of Sciences & Yunnan Province, Kunming Institute of Zoology, Kunming, Yunnan, 650223, China

Center for Excellence in Animal Evolution and Genetics, Chinese Academy of Sciences, Kunming, Yunnan, 650223, China

Kunming College of Life Science, University of Chinese Academy of Sciences, Kunming, Yunnan, 650204, China

KIZ – CUHK Joint Laboratory of Bioresources and Molecular Research in Common Diseases, Kunming Institute of Zoology, Chinese Academy of Sciences, Kunming, Yunnan, 650223, China

* Corresponding author.
E-mail address: yaoyg@mail.kiz.ac.cn (Y.-G. Yao).

22 August 2019
Available online 5 November 2019

Supplementary Data

This supplementary file contains 1 Online Materials and Methods, 1 supplementary Reference section, 5 supplementary tables (Tables S1-S5), and 4 supplementary figures (Figures S1-S4).

1. Materials and methods

1.1 Modeling analysis of the PSSs

The *MDA5* and *LGP2* genes of chicken, mallard, zebrafish, dog and cow (Table S1) were retrieved from Ensembl (http://asia.ensembl.org/index.html) to test for potentially selective pressure in the chicken lineage. We followed the same procedure described in our previous studies (Fan *et al.*, 2018; Fan *et al.*, 2014; Xu *et al.*, 2016). Briefly, the branch model tests were implemented by using the CODEML program in the PAML package (Yang, 2007) to calculate the average non-synonymous substitution/ synonymous substitution rate (dN/dS, also known as ω). The one-ratio model (M0) with the same ω for all branches and the two-ratio model (M2) with different ω on the foreground branches were used to calculate the likelihood values of M0 and M2. The branch-site model tests were also implemented by using the CODEML program in the PAML package (Yang 2007) to estimate different ω values among the branches and sites, which allows for 3 category sites (purifying, neutral and positive selection) with different ω values in foreground branch, whereas background branches only have 2 category sites (purifying and neutral). The likelihood values of the two models are computed: a null model (H0), in which the foreground branch may have different proportions of sites under neutral selection, and an alternative model (H1), in which the foreground branch may have a proportion of sites under positive selection (Yang 2007). Finally, the likelihood ratio test (LRT) was performed to judge which model should be selected (Zhang *et al.*, 2005).

1.2 Viruses and cell lines

The HEK293 and DF-1 cells were purchased from the Kunming Cell Bank, Kunming Institute of Zoology, and were grown in high-glucose Dulbecco's modified eagle medium (DMEM; Gibco-BRL, 11965-092) supplemented with 10% (vol / vol) fetal bovine serum (FBS; Gibco-BRL, 10099-141) and 1× penicillin/streptomycin (Gibco-BRL, 10378016) at 37 ^{o}C in 5% CO_2.

The Newcastle disease virus (NDV) and avian influenza virus (AIV) were propagated and amplified as previously described (Xu *et al.*, 2015). The DF-1 and HEK293 cells were incubated with or without NDV (MOI [multiplicity of infection] = 1), AIV (MOI=1) for 1 h in DMEM without FBS. The cells were then rinsed and cultured in fresh DMEM containing 1% (vol / vol) FBS for different time intervals before harvest.

1.3 Reverse transcription quantitative real-time PCR (RT-qPCR)

Total RNA was extracted from the DF-1 cells using the RNAsimple Total RNA Kit (TIANGEN, Beijing, DP419) according to the manufacturer's instructions. The A260/A280 ratio of total RNA was measured on a NanoDrop biophotometer (Thermo Fisher Scientific Inc., DE, USA) and only these samples with a value of 1.8-2.0 were used for subsequent reverse transcription. We also evaluated the quality and integrity of the RNA samples based on the 28S and 18S rRNA bands using 1% agarose gel. Around 1 μg total RNA was used to synthesize cDNA by using oligo-dT_{18} primer and M-MLV reverse transcriptase (Promega, USA, M1701). RT-qPCR was performed using SYBR green Premix Ex Taq II (TaKaRa, Dalian, China, RR820L) supplemented with gene specific primers (Table S5) on a MyIQ2 Two-Color Real-Time PCR Detection system (Bio-Rad Laboratories, Hercules, CA, USA), as described previously (Xu et al., 2015; Yu *et al.*, 2014) . We serially diluted the PCR product of the *chIFNB1* amplicon and used the 10^{-3} - 10^{-10} dilutions to generate the standard curve for quantifying the level of *chIFNB1* mRNA. The Ct values were

measured relative to the corresponding standard curve. The chicken housekeeping gene *GAPDH* (*chGAPDH*) was used as the reference for normalization (Table S5).

1.4 Luciferase reporter assay

The chMDA5, chLGP2, chSTING and chIFN-β-Luc reporter (chIFN-β-Luc) constructs were kind gifts from Dr. Ze-Qing Feng. Human IFN-β-Luc, NF-κB-Luc and ISRE-Luc, ISRE-Luc and TK were reported as previously (Xu et al., 2016). All the chMDA5, chLGP2, hMDA5 and hLGP2 mutants were generated by multi-sites directed mutagenesis (Stratagene, USA, 200518; Table S5). For transfection, the DF-1 cells were plated in 24-well plates at a density of 1×10^4 cells and cultured overnight. Cells were transfected with 0.1 μg of each luciferase reporter vector (chIFN-β-Luc, NFκB-Luc, IFN-β-Luc and ISRE-Luc), together with 0.01 μg pRL-SV40-*Renilla* (TK; as an internal control), the indicated amount of an empty vector (Mock) or indicated expression vector by using Lipofectamine™ 3000 (Invitrogen, USA, 11668-027). The transfected cells were left untreated or infected with NDV (MOI = 1) for 12 h. Cells were harvested and luciferase activity was measured using the Dual-Luciferase Reporter Assay System (Promega, USA, E1960) on Infinite M1000 Pro multimode microplate reader (Tecan, USA, 30064852).

1.5 Western blot and immunoprecipitation

The DF-1 cells were seeded in 6-well plates to grow to 70% confluence and were transfected using X-tremeGENE HP DNA Transfection Reagent (Roche, USA, 06366546001). Cells were lysed on ice in RIPA lysis buffer (Beyotime Institute of Biotechnology, P0013). After centrifugation at 12,000 × g at 4 °C for 5 min, cell lysates were separated by electrophoresis on 12% (vol/vol) sodium dodecyl sulfate (SDS)-polyacrylamide gel and transferred to polyvinylidene fluoride (PVDF) membranes (Roche Diagnostics, IPVH00010) using standard procedures. The membranes were soaked in the blocking buffer [5% (wt/vol) skimmed milk or 5% (wt/vol) bovine serum albumin in TBST (Tris Buffered Saline (Cell Signaling Technology, 9997) with Tween 20 (0.1%; Sigma, P1379)) at room temperature for 2 h. The membranes were then incubated with the indicated primary antibodies overnight at 4 °C: mouse monoclonal anti-Flag (1: 5000; Abmart, M20008), mouse anti-Myc (9E11) (1:5000; Life Technologies, MA1-16637), mouse monoclonal anti-HA (1:5000; EnoGene, E12-003-4) and mouse monoclonal anti β-actin (1:10000, Enogene), respectively. After washing with 1× TBST for three times (5 min each), membranes were incubated with TBST-conjugated anti-mouse (KPL, 474-1806) or anti-rabbit (KPL, 074-1506) secondary antibody (depends on the primary antibody; 1:10000, KPL, USA) for 1 h at room temperature. After another round of three washes with TBST, the membranes were examined using enhanced chemiluminescence (ECL) reagents (Millipore, WBKLS0500). ImageJ (National Institutes of Health, Bethesda, Maryland, USA) was used to evaluate the densitometry.

For immunoprecipitation, appropriate antibodies were incubated with protein G-agarose beads (Life Technologies, USA, 15920010) for 1 h. At the same time, cells were lysed with RIPA lysis buffer (Beyotime Institute of Biotechnology, P0013) on ice for 1 h, followed by a centrifugation at 12,000 × g for 10 min. Lysates were precipitated with the above beads-antibody complexes at 4 °C overnight, followed by washing with the RIPA lysis buffer (Beyotime, P0013) before being re-suspended in loading sample buffer for SDS-PAGE. The chMDA5 and chLGP2 immunoprecipitation assays were performed using the procedures as previously reported (Deddouche *et al.*, 2014; Xu et al., 2016). Briefly, about 1.5×10^8 cells were transfected with 30 μg of HA-tagged chMDA5 or/and Myc-tagged chLGP2 plasmid using X-tremeGENE HP DNA Transfection Reagent following the manufacturer instructions. Cells were incubated for 24 h in growth medium and then infected with NDV (MOI=1) for 16 h. The subsequent procedure was fully described by previous studies (Deddouche et al., 2014; Xu et al., 2016). Briefly, cells were washed and lysed in the lysis buffer (10 mM Tris pH 7.4, 2.5 mM MgCl2, 200 mM NaCl, 0.5% NP40, 1×protease inhibitor cocktail (Millipore, USA, 539131), 0.5 U/ml RNasin (Promega, USA, N2111)). A small fraction of the input was collected for protein and RNA extraction. About 5 μg of indicated primary antibody or mouse IgG isotype control antibody (Beyotime Institute of Biotechnology, A7028) was added to 500 μL of lysate and incubated on a rotating shaker for 1 h at 4°C. The Gamma Bind Plus Sepharose Beads (300 μL; GE Healthcare Bioscience AB, 10004D) were washed with the lysis buffer and added to the lysate-primary antibody mixture for another 1

h. The beads were precipitated by centrifugation (7000 g for 1 min) and washed 4 times with 1 mL of lysis buffer and divided in two proportions for protein and RNA extraction. The beads were boiled for 5 min in SDS sample buffer to extract protein from the protein-RNA complexes for Western blot analysis. RNAs were purified from the beads by using TRIzol (Invitrogen, USA, 15596018).

1.6 Statistical test

The differences of relative levels of mRNA and luciferase activities between the groups with different treatments were calculated by using the two-tailed Student's *t* test (PRISM software, GraphPad Software, Inc., La Jolla, CA, USA). Data was represented as mean±SEM, with a *P* value < 0.05 considered to be significant.

2. Supplementary Tables

Table S1. The MDA5 and LGP2 sequences used for the positive selection analyses

Species	Common name	MDA5 accession number	LGP2 accession number
Gallus gallus	Chicken	ENSGALG00000041192	ENSGALG00000023821
Anas platyrhynchos	Mallard	ENSAPLG00000010913	ENSAPLG00000013187
Danio rerio	Zebrafish	ENSDARG00000018553	ENSDARG00000089463
Canis familiaris	Dog	ENSCAFG00000010438	ENSCAFG0000001572
Bos taurus	Cow	ENSBTAG00000008142	ENSBTAG00000046580

Note: Sequence accession numbers were referred to the Ensemble database (http://asia.ensembl.org/index.html).

Table S2. Branch model analysis for positive selection on the *MDA5* and *LGP2* genes in the chicken lineage

Gene	lnL (null)[a]	np1[b]	lnL (alternative)	np2	*P*-value	Parameters
MDA5	-14572.1	17	-14569.1	18	**0.014**	M0: All branches have the same $\omega_0 = 0.19018$ M2: The tree shrew branch has $\omega_2 = 0.31887$, other branches have $\omega_1 = 0.18143$
LGP2	-11701.8	19	-11700.9	20	0.191	M0: All branches have the same $\omega_0 = 0.13062$ M2: The tree shrew branch has $\omega_2 = 0.10244$, other branches have $\omega_1 = 0.13474$

A *P*-value < 0.05 was regarded as significant and marked in bold.
[a] lnL: log-likelihood value.
[b] np: Number of parameters. The np1 is the number of parameters under the null model; the np2 is the number of parameters under the alternative model.

Table S3. Analysis of the positive selection on the *MDA5* and *LGP2* genes of the chicken lineage using the branch-site model

Foreground	lnL [a] (null)	np1[b]	lnL[a] (alternative)	np2[b]	2ΔlnL[c]	*P*-value [c]	Positively selected sites	Parameters [d]			
MDA5	-15616.0	19	-15616.0	20	0	1	99 C 0.588, 305 G 0.503, 409 E 0.555, 445 S 0.523, 485 Q 0.577, **625 L 0.970**, 752 H 0.546, 769 F 0.507, 898 V 0.503	p_0=0.66788	p_1=0.25628	p_{2a} =0.05481	p_{2b}=0.02103
								ω_0=0.07078	ω_1=1.00000	ω_2=1.00000	
LGP2	-11720.2	21	-11717.4	22	5.651	**0.017**	**404 S 0.938**, **661 S 0.893**, **672 E 0.945**	p_0=0.74192	p_1=0.22465	p_{2a} =0.02567	p_{2b}=0.00777
								ω_0=0.06489	ω_1=1.00000	ω_2=1.35837	

[a] lnL: log-likelihood value.
[b] np: Number of parameters. The np1 is the number of parameters under the null model; the np2 is the number of parameters under the alternative model.
[c] For each model, we get the log likelihood value (alternative model and null model), from which we compute the Likelihood Ratio Test (LRT). Twice the difference of log likelihood values (2ΔlnL) between the two models was compared. The 2ΔlnL follows a χ^2 curve with degree of freedom of 1, so we can get a *P*-value for this LRT. The positively selected sites were estimated using the BEB analysis.
[d] ω_0 - the ω value of purifying selection sites; ω_1 - the ω value of neutral evolution sites; ω_2 - the ω value of positive selection sites; p_0 - proportion of sites that are under purifying selection ($\omega_0 < 1$) on both foreground and background branches; p_1 - proportion of sites that are under neutral evolution ($\omega_1 = 1$) on both foreground and background branches; p_{2a} - proportion of sites that are under positive selection ($\omega_2 \geq 1$) on the foreground branch and under purifying selection ($\omega_0 < 1$) on background branches; p_{2b} - proportion of sites that are under positive selection ($\omega_2 \geq 1$) on the foreground branch and under neutral evolution ($\omega_1 = 1$) on background branches.

Table S4. Mutations in the equivalent positively selected sites of *MDA5* and *LGP2* in human populations

MDA5	Population	187th residue	405th residue	p.Glu633Asp[a]
Public data	ExAC (East Asian)	0	0	23/8568 (0.0027)
	COSMIC	0	0	0
	CMDB (Chinese)	0	0	43/14007 (0.0031)
LGP2	Population	406th residue	663rd residue	675th residue
Public data	ExAC (East Asian)	0	0	0
	COSMIC	0	0	0
	CMDB (Chinese)	0	0	0

[a] Allele count / total allele number (minor allele frequency)

Data resources: the Exome Aggregation Consortium (ExAC, http://exac.broadinstitute.org/) is a collection of exome sequencing data from a variety of large-scale sequencing projects (Walsh *et al.*, 2017).

Catalogue of somatic mutations in cancer (COSMIC, http://cancer.sanger.ac.uk/cosmic) is designed to store and display somatic mutation information, with the largest sample size of human cancer studies (Forbes *et al.*, 2016).

The Chinese Millionome Database (CMDB, https://db.cngb.org/cmdb/) is a large-scale Chinese genomics database (n= 141,431 individuals) produced by BGI and hosted by the National GeneBank (Liu *et al.*, 2018).

Table S5. Primers and vectors used in this study

Primer	Sequence (5'-3')	Application and vector
chIFNB1-qF	CCTCAACCAGATCCAGCATTAC	Analytical quantitative real-time PCR (RT-qPCR)
chIFNB1-qR	CCCAGGTACAAGCACTGTAGTT	
chGAPDH-qF	AGGACCAGGTTGTCTCCTGT	Analytical RT-qPCR
chGAPDH-qR	CCATCAAGTCCACAACACGG	
chMDA5 L625E-F	TATAAGGAGGAAAAAAGGAGGAAGAC	PCR for constructing mutant chMDA5 L625E based in chMDA5 expression vector
chMDA5 L625E-R	GTCTTCCTCCTTTTTTCCTCCTTATA	
chLGP2 S404A-F	CGGTGCCGGCCACAGCAACCAG	PCR for constructing mutant chLGP2 S404A based in chLGP2 expression vector
chLGP2 S404A-R	CTGGTTGCTGTGGCCGGCACCG	
chLGP2 S661D-F	GAGGAGTTCGACTACCTGGAGTACTG	PCR for constructing mutant chLGP2 S661D based in chLGP2 expression vector
chLGP2 S661D-R	CAGTACTCCAGGTAGTCGAACTCCTC	
chLGP2 E672L-F	CTGCTCCAGCACTCAGGACCUGTCCC	PCR for constructing mutant chLGP2 E672L based in chLGP2 expression vector
chLGP2 E672L-R	GGGACAGGUCCUGAGUGCUGGAGCAG	
hMDA5 E633L-F	CTATAATGAACTGAAAGATAAGAAGTTTGC	PCR for constructing mutant hMDA5 E633L based in hMDA5 expression vector
hMDA5 E633L-R	GCAAACTTCTTATCTTTCAGTTCATTATAG	
hLGP2-EcoRI –F	AG***GAATTC***TCATGGAGCTTCGGTCCTAC	PCR for constructing HA-tagged hLGP2 expression vector based on pCMV-HA vector using
hLGP2-BglII-R	GA***AGATCT***CTCAGTCCAGGGAGAGGTCCG	*Eco*R I and *Bgl* II
hLGP2 A406S-F	GGGAGTGGGAACAGCAGCCAGAGCACC	PCR for constructing mutant hLGP2 A406S based in hLGP2 expression vector
hLGP2 A406S-R	GGTGCTCTGGCTGCTGTTCCCACTCCC	
hLGP2 D663S-F	CTGACTTTAGCTTCCTGCAGCATTGTG	PCR for constructing mutant hLGP2 D663S based in hLGP2 expression vector
hLGP2 D663S-R	CACAATGCTGCAGGAAGCTAAAGTCAG	
hLGP2 L675E-F	AACTTGTCGGACCTCTCCCTGGACTG	PCR for constructing mutant hLGP2 L675E based in hLGP2 expression vector
hLGP2 L675E-R	TCAGTCCAGGGAGAGGTCCGACAAGT	

3. Supplementary Figures

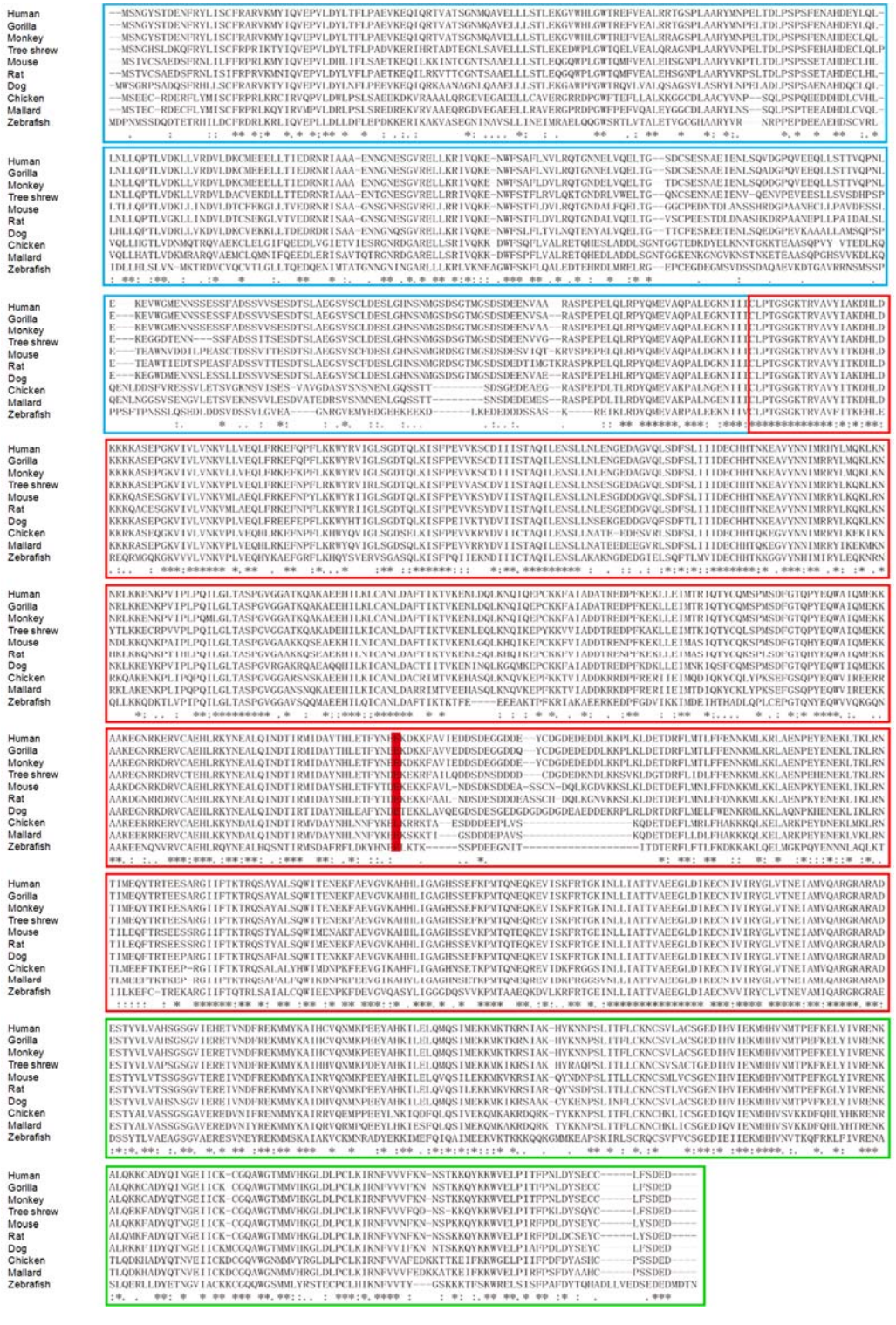

Fig. S1. Protein sequence alignment of part of the DECH Box Helicase domain in 10 vertebrate species (human (ENSG00000115267), gorilla (ENSGGOT00000015950), rhesus monkey (ENSMMUG00000003202), tree shrew (XM_006160265.3), rat (ENSRNOG00000006227), mouse (ENSMUSG00000026896), dog, chicken, mallard and zebrafish; Table S1)). Outline boxes in blue, red and green delimit the CARD, DECH-box helicase domain and CTD domains. The positively selected site is marked in red. These sequences were alignment by using MUSCLE program (http://www.drive5.com/muscle/) (Edgar, 2004).

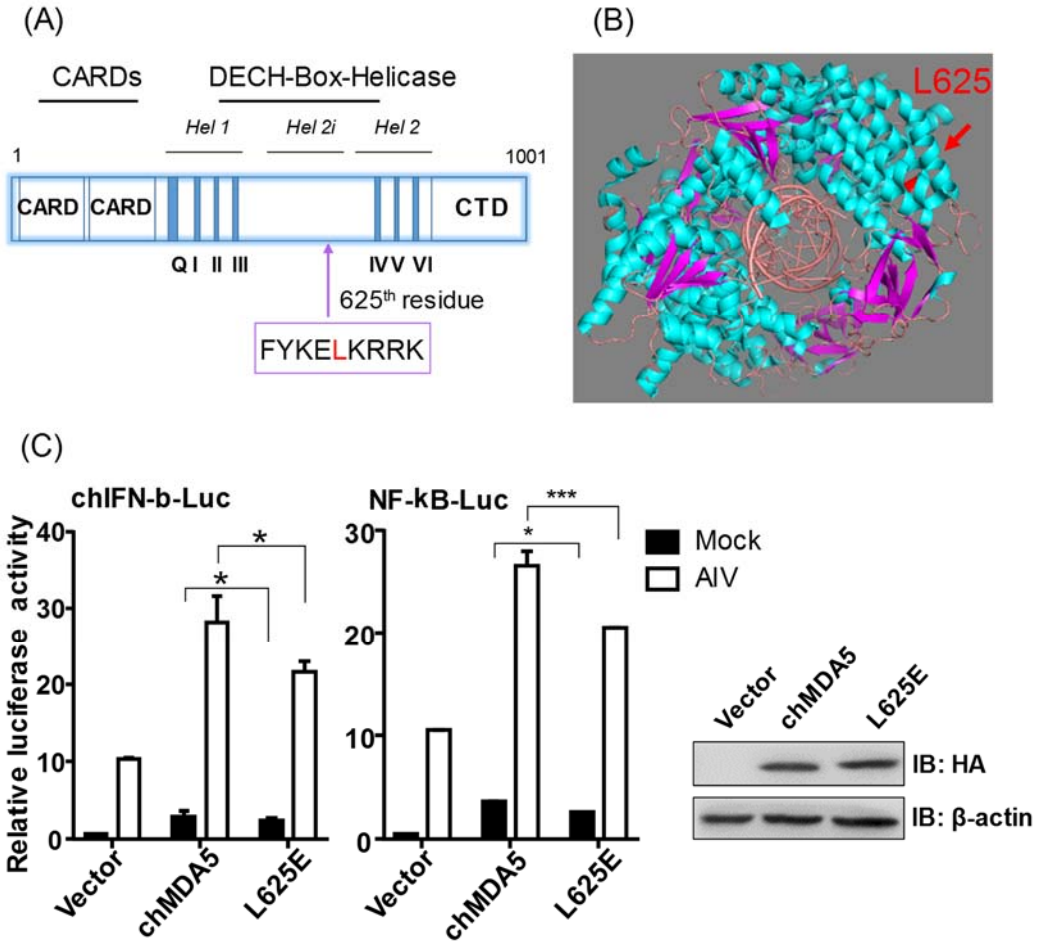

Fig. S2. Evolution of the positively selected site in the chicken MDA5 and its impact on the predicted protein structure.
(A) Diagram illustrating domain structure and feature of the chicken MDA5 (chMDA5). The chMDA5 are composed of three critical domains: (1) tandem caspase activation and recruitment domains (CARD) at its N-terminal, which are essential for interactions with MAVS to promote downstream signaling; (2) a central DECH-box helicase domain that encompasses conserved helicase sub-domains, Hel1 (surrounding helicase motifs Q, I, II and III), Hel2 (surrounding helicase motifs IV, V, and VI), and the helicase insert domain Hel2i; and (3) a C-terminal domain (CTD) for auto-regulation and RNA terminus recognition.
(B) Predicted structure of chMDA5-dsRNA (PBD: 5jc3) to show the equivalent position of the positively selected site L625 (marked in red arrow) in chicken.
(C) Different activation effects of chMDA5 and its mutant on the chIFN-β-Luc and NF-κB-Luc reporters in response to AIV infection. (*Left*) The DF-1 cells (1×10^4) were transfected with the respective reporter vector (100 ng), TK (10 ng, as an inner control) and the indicated expression vector (400 ng) for 36 h, then were left uninfected or infected with AIV (MOI=1) for 12 h before the harvest for luciferase analysis. (*Right*) Immunoblots showing successful overexpression of HA-tagged chMDA5 and its mutant L625E.
Data are representative of three independent experiments. * $P < 0.05$, *** $P<0.0001$, Student's *t* test. Bars represent mean ± SEM.

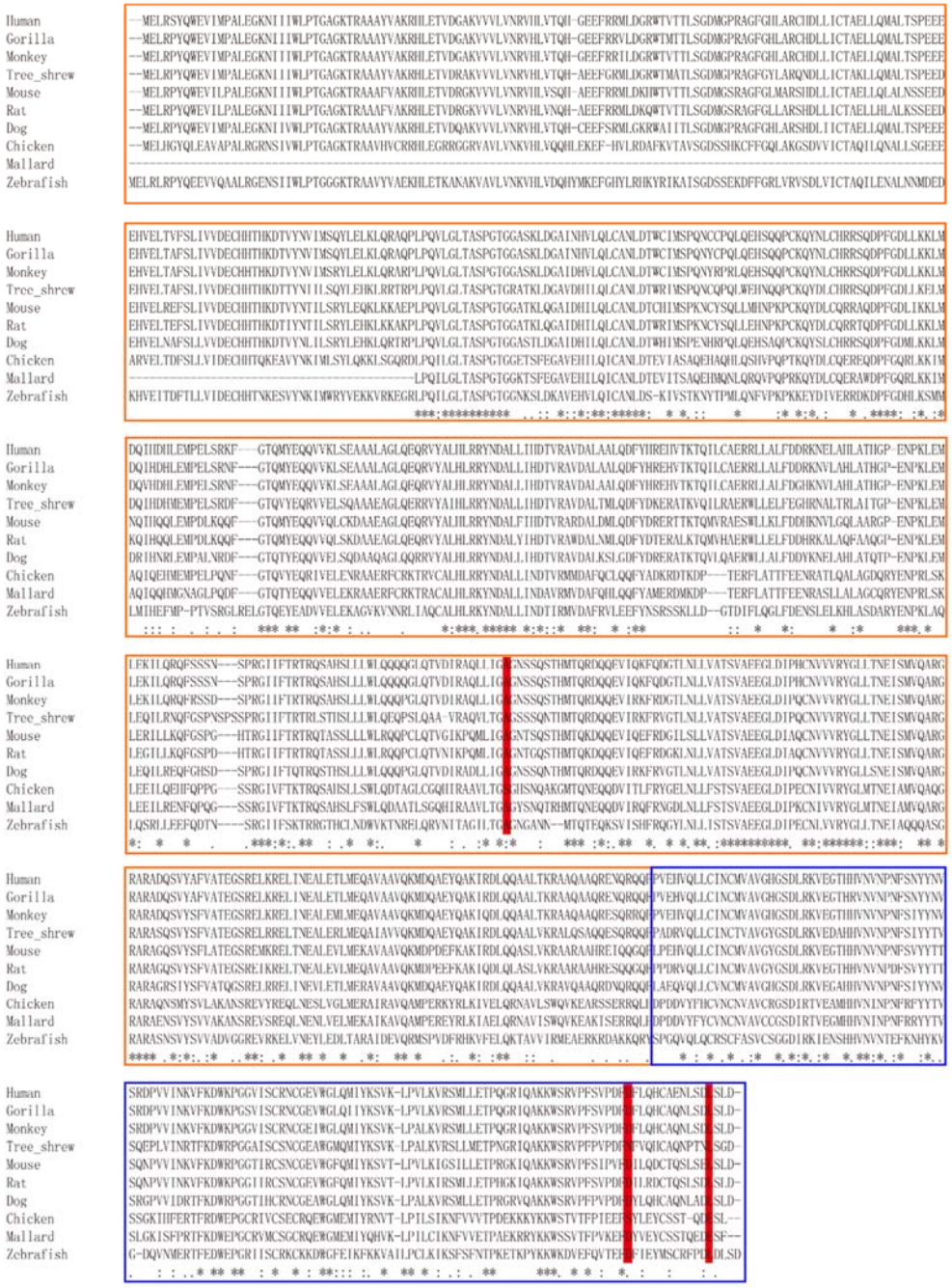

Fig. S3. Protein sequence alignment of part of the DECH-box helicase and CTD domain in 10 vertebrate (human (ENSG00000108771), gorilla (XM_004041703), rhesus monkey (ENSMMUG000000147), tree shrew (XM_027774775), rat (ENSRNOG00000018247), mouse (ENSMUSG00000017830), dog, chicken, mallard and zebrafish; Table S1). Outline boxes in red and blue delimit the DECH-box helicase domain and RD domains. The positively selected sites are marked in red. These sequences were alignment by using MUSCLE program.

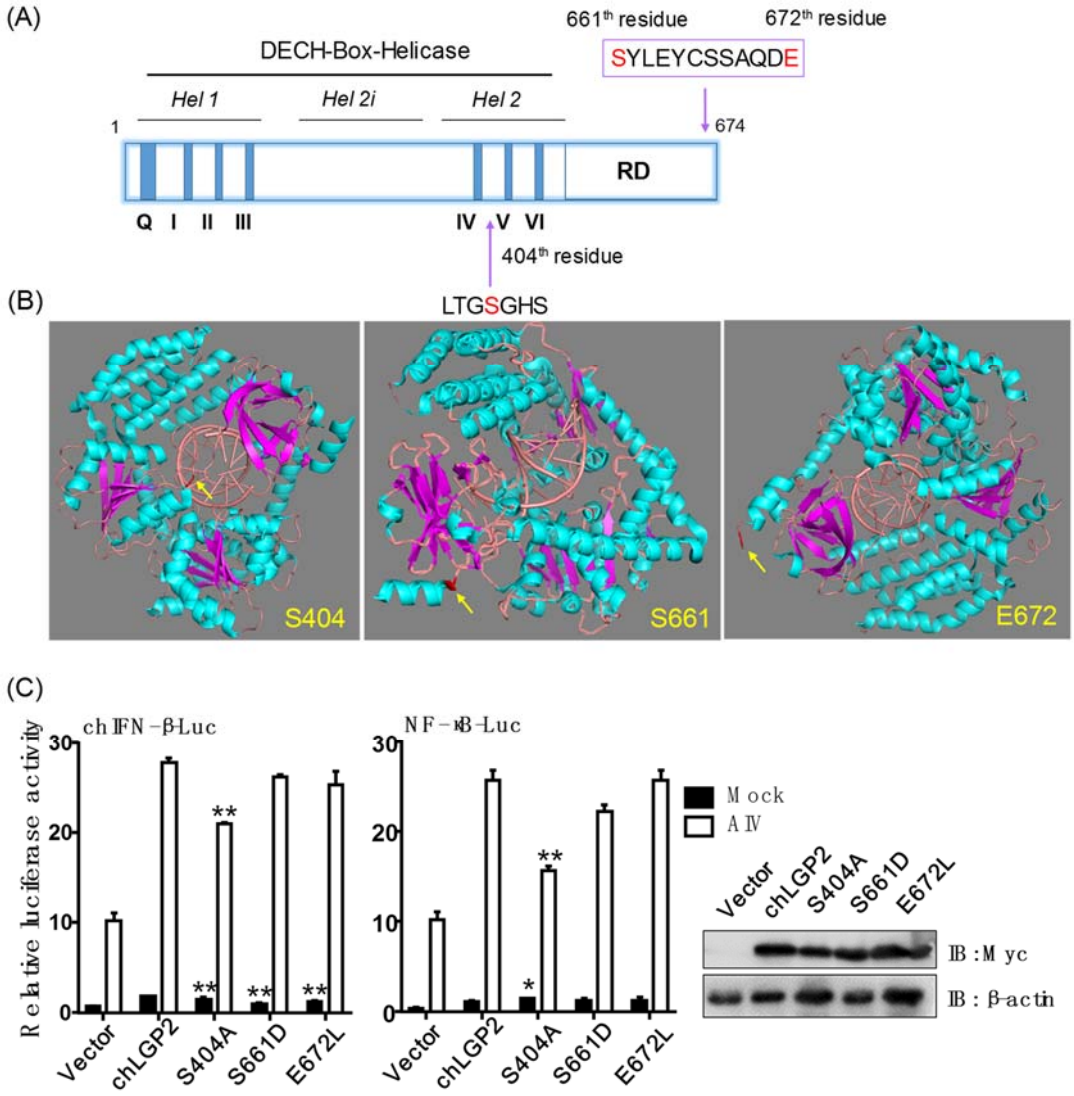

Fig. S4. Evolution of the positively selected sites in the chicken LGP2 and its impact on the predicted protein structure.
(A) Diagram illustrating domain structure and feature of the chicken LGP2 (chLGP2). The chLGP2 are composed of two critical domains: (1) a DECH-box helicase domain that encompasses conserved helicase sub-domains, Hel1 (surrounding helicase motifs Q, I, II and III), Hel2 (surrounding helicase motifs IV, V, and VI), and the helicase insert domain Hel2i; and (2) a repression domain (RD) for auto-regulation and RNA terminus recognition.
(B) Predicted structures of chLGP2 binding with dsRNA (PBD: 5jaj) to show the equivalent position of the positively selected sites (marked in yellow arrows) in chicken.
(C) Different activation effects of chLGP2 and its mutants on the chIFN-β-Luc and NF-κB-Luc reporters. (*Left*) The DF-1 cells (1×10^4) were transfected with the respective reporter vector (100 ng), TK (10 ng, as an inner control) and the indicated expression vector (400 ng) for 36 h, then were left uninfected or infected with AIV (MOI=1) for 12 h before the harvest for luciferase analysis. (*Right*) Immunoblots showing successful overexpression of Myc-tagged chLGP2 and its mutants. * $P < 0.05$, ** $P < 0.01$, relative to the chLGP2 group for each comparison of the mock or the AIV infection.

4. References

Deddouche, S., Goubau, D., Rehwinkel, J., Chakravarty, P., Begum, S., Maillard, P.V., Borg, A., Matthews, N., Feng, Q., van Kuppeveld, F.J.M., Reis e Sousa, C., and Chen, Z.J. 2014. Identification of an LGP2-associated MDA5 agonist in picornavirus-infected cells. eLife 3, e01535.

Edgar, R.C. 2004. MUSCLE: multiple sequence alignment with high accuracy and high throughput. Nucleic Acids Res. 32, 1792-1797.

Fan, Y., Luo, R., Su, L.Y., Xiang, Q., Yu, D., Xu, L., Chen, J.Q., Bi, R., Wu, D.D., Zheng, P., and Yao, Y.G. 2018. Does the genetic feature of the Chinese tree shrew (*Tupaia belangeri chinensis*) support its potential as a viable model for Alzheimer's disease research? J. Alzheimers Dis. 61, 1015-1028.

Fan, Y., Yu, D.D., and Yao, Y.G. 2014. Positively selected genes of the Chinese tree shrew (*Tupaia belangeri chinensis*) locomotion system. Zool. Res. 35, 240-248.

Forbes, S.A., Beare, D., Bindal, N., Bamford, S., Ward, S., Cole, C.G., Jia, M., Kok, C., Boutselakis, H., De, T., Sondka, Z., Ponting, L., Stefancsik, R., Harsha, B., Tate, J., Dawson, E., Thompson, S., Jubb, H., and Campbell, P.J. 2016. COSMIC: high-resolution cancer genetics using the catalogue of somatic mutations in cancer. Curr. Protoc. Hum. Genet. 91, 10.11.11-10.11.37.

Liu, S., Huang, S., Chen, F., Zhao, L., Yuan, Y., Francis, S.S., Fang, L., Li, Z., Lin, L., Liu, R., Zhang, Y., Xu, H., Li, S., Zhou, Y., Davies, R.W., Liu, Q., Walters, R.G., Lin, K., Ju, J., Korneliussen, T., Yang, M.A., Fu, Q., Wang, J., Zhou, L., Krogh, A., Zhang, H., Wang, W., Chen, Z., Cai, Z., Yin, Y., Yang, H., Mao, M., Shendure, J., Wang, J., Albrechtsen, A., Jin, X., Nielsen, R., and Xu, X. 2018. Genomic analyses fromnon-invasive prenatal testing reveal genetic associations, patterns of viral infections, and Chinese population history. Cell 175, 347-359.e314.

Walsh, R., Thomson, K.L., Ware, J.S., Funke, B.H., Woodley, J., McGuire, K.J., Mazzarotto, F., Blair, E., Seller, A., Taylor, J.C., Minikel, E.V., Exome Aggregation, C., MacArthur, D.G., Farrall, M., Cook, S.A., and Watkins, H. 2017. Reassessment of Mendelian gene pathogenicity using 7,855 cardiomyopathy cases and 60,706 reference samples. Genet. Med. 19, 192-203.

Xu, L., Yu, D., Fan, Y., Peng, L., Wu, Y., and Yao, Y.G. 2016. Loss of RIG-I leads to a functional replacement with MDA5 in the Chinese tree shrew. Proc. Natl. Acad. Sci. U. S. A. 113, 10950-10955.

Xu, L., Yu, D., Peng, L., Fan, Y., Chen, J., Zheng, Y.-T., Wang, C., and Yao, Y.-G. 2015. Characterization of a MAVS ortholog from the Chinese tree shrew (*Tupaia belangeri chinensis*). Dev. Comp. Immunol. 52, 58-68.

Yang, Z. 2007. PAML 4: phylogenetic analysis by maximum likelihood. Mol. Biol. Evol. 24, 1586-1591.

Yu, D., Xu, L., Liu, X.-H., Fan, Y., Lü, L.-B., and Yao, Y.-G. 2014. Diverse interleukin-7 mRNA transcripts in Chinese tree shrew (*Tupaia belangeri chinensis*). PLoS One 9, e99859.

Zhang, J., Nielsen, R., and Yang, Z. 2005. Evaluation of an improved branch-site likelihood method for detecting positive selection at the molecular level. Mol. Biol. Evol. 22, 2472-2479.